Effects of Remote Boundary Conditions on Clamping Loss in Micromechanical Resonators

James M. L. Miller[®], Gabrielle D. Vukasin[®], Ze Zhang, Hyun-Keun Kwon[®], Arun Majumdar, Thomas W. Kenny, and Steven W. Shaw[®]

Abstract-Clamping loss in micromechanical resonators can strongly depend on the boundary conditions far away from the actual vibrating structure because the acoustic wavelength greatly exceeds the device dimensions. We demonstrate a scheme for post-fabrication tuning of the clamping loss in flexural-mode and bulk-mode resonators by modifying the boundary conditions of the chip with the frame. The measured quality factor increases by more than an order-of-magnitude for the microcantilevers and more than a factor of three for the bulk-mode resonators when frame contact is minimized via suspension of the chip by wirebonds. We propose a two-degree-of-freedom fluctuationdissipation model to describe the thermomechanical noise and forced response in the presence of this tunable anchor damping. By studying the thermomechanical displacement spectrum with tunable clamping loss, we show that variable clamping loss tunes the mechanical quality factor, modifying both the resonator transfer function and thermomechanical noise force. We delineate the dependence of the tunable clamping loss mechanism on microcantilever beam length and ambient temperature from 300 K down to 40 K, and observe potential temperature dependence to clamping loss with reducing temperature. [2021-0141]

Index Terms—MEMS, microresonators, clamping loss, anchor damping, thermoelastic dissipation, fluctuation-dissipation theorem.

Manuscript received June 30, 2021; revised December 7, 2021; accepted December 14, 2021. Date of publication January 7, 2022; date of current version April 4, 2022. This work was supported in part by the National Science Foundation Collaborative Research Program under Award CMMI-1662619 and Award CMMI-1662464; and in part by the National Science Foundation (NSF) as a part of the National Nanotechnology Coordinated Infrastructure through the Defense Advanced Research Projects Agency Precise Robust Inertial Guidance for Munitions (PRIGM) Program, managed by Ron Polcawich and Robert Lutwak, under Award ECCS-1542152. The work of Steven W. Shaw was supported by NSF under Award CMMI-1662619 and Award CMMI-1561829. Subject Editor R. N. Candler. (Corresponding authors: James M. L. Miller; Gabrielle D. Vukasin.)

James M. L. Miller is with the Department of Mechanical and Civil Engineering, Florida Institute of Technology, Melbourne, Fl. 32901 USA, also with the Department of Mechanical Engineering and the Department of Physics and Astronomy, Michigan State University, East Lansing, MI 48823 USA, and also with the Department of Mechanical Engineering and the Department of Electrical Engineering, Stanford University, Stanford, CA 94305 USA (e-mail: jmln@illinois.edu).

Gabrielle D. Vukasin, Ze Zhang, Hyun-Keun Kwon, Arun Majumdar, and Thomas W. Kenny are with the Department of Mechanical Engineering and the Department of Electrical Engineering, Stanford University, Stanford, CA 94305 USA (e-mail: gvukasin@stanford.edu; tkenny@stanford.edu).

Steven W. Shaw is with the Department of Mechanical and Civil Engineering, Florida Institute of Technology, Melbourne, FL 32901 USA, and also with the Department of Mechanical Engineering and the Department of Physics and Astronomy, Michigan State University, East Lansing, MI 48823 USA (e-mail: sshaw@fit.edu).

Color versions of one or more figures in this article are available at https://doi.org/10.1109/JMEMS.2021.3136885.

Digital Object Identifier 10.1109/JMEMS.2021.3136885

I. INTRODUCTION

ICRO- and nanoelectromechanical (MEM/NEM) resonators are widely used in sensors [1] and oscillators [2]. Perhaps the most important attribute in MEM/NEM resonators is the quality factor, Q, which characterizes the dissipation in the mechanical mode. A variety of dissipation mechanisms contribute to determining the Q in MEM/NEM resonators, such as clamping loss (Q_{clamp}), thermoelastic dissipation (Q_{TED}), surface loss (Q_{surf}), gas damping (Q_{gas}), and phonon loss (Q_{phon}). These mechanisms are linked to the mechanical quality factor of the resonator, and thus their tuning modifies both the transfer function and thermomechanical noise force acting on the resonator. The quality factors associated with these dissipation mechanisms sum in inverse to determine the total inverse mechanical quality factor:

$$\frac{1}{Q} = \frac{1}{Q_{clamp}} + \frac{1}{Q_{TED}} + \frac{1}{Q_{surf}} + \frac{1}{Q_{gas}} + \frac{1}{Q_{phon}} + \cdots$$

$$\tag{1}$$

The mechanical quality factor Q is determined by the various actual dissipation mechanisms in Eq. 1. In contrast to Q, a variety of feedback or pumping techniques have been developed to tune the "effective" quality factor, Q_{eff} [3]. Effective quality factor tuning modifies the resonator dynamics by pulling energy out of or feeding energy into the mode, resulting in modal "cooling" or "heating" [4]–[8]. If sufficient energy is fed into the mode, Q_{eff}^{-1} becomes negative and self-sustained oscillations commence [9]-[12]. During selfsustained oscillations, the nonlinearities govern the vibrational response [13]-[17]. Q_{eff} tuning has no influence on the thermomechanical noise force that acts on the resonator; this noise force has a white amplitude spectral density F_{th} = $\sqrt{4k_BTm\omega_0Q^{-1}}$, where Q is the mechanical quality factor, $k_B = 1.3807 \times 10^{-23} \text{ J K}^{-1}$ is Boltzmann's constant, T is the thermal bath temperature, ω_0 is the modal angular resonance frequency, and m is the modal lumped mass. In contrast, the larger the mechanical quality factor (Q), the weaker the coupling between the mode and the thermal bath, resulting in a weaker thermomechanical noise force acting on the mode and typically a better signal-to-noise ratio (SNR) for the corresponding resonant sensor or oscillator.

Clamping loss (also known as anchor loss or support loss) occurs when elastic energy in the resonator radiates through the supports into the substrate. Clamping loss is often a dominant damping mechanism in MEM/NEM resonators, degrading

Q and resulting in a larger thermomechanical noise force. The earliest resonator innovation which reduced clamping loss was the double-ended tuning fork design for musical instruments. The out-of-phase mode of the two vibrating elements in a DETF have zero net force and moment at the supports, which results in a significantly higher Q value than a corresponding cantilever of similar dimensions due to reduced clamping loss [18]. More recent innovations for reducing clamping loss include engineering the tether geometry [19]–[32] and integrating phononic crystals into the resonator or anchors [33]–[53].

Because the wavelengths of acoustic waves at radiofrequencies are often much larger than the MEM/NEM resonators that radiate them, the boundary conditions away from the actual vibrating structures can also influence the clamping loss. Preliminary measurements in this direction suggest that chip mounting conditions do influence clamping loss in silicon nitride membranes [54], [55] and double-ended tuning forks [56], [57]. The advantage of modifying the chip mounting conditions over the phononic crystal or engineered tether methods is that it enables post-fabrication tuning of clamping loss [58]. This is useful for increasing the post-fabrication mechanical quality factor of doubly-clamped beams [20], thermal-piezoresistive oscillators [6], [59]-[63], and other resonator geometries that require multiple attachment points via rigid anchor tethers. The boundary-condition-dependence is also important because many computational models for clamping loss rely on energy loss through a perfectly-matched layer, which do not necessarily properly account for interfaces at the boundary of the chip, and are thus unlikely to provide accurate predictions of clamping loss [29], [56]. In this work, we experimentally show that modifying the post-fabrication chip-substrate boundary conditions can tune the clamping loss by over an order-of-magnitude. The chip-frame boundary conditions are important because the acoustic wavelength of vibrations can dramatically exceed the size of the chip for micromechanical resonators vibrating at radiofrequencies, as illustrated in Table I.

II. THE DEVICES

This Article experimentally studies the influence of remote boundary conditions on radiofrequency clamping loss in micromechanical flexural-mode and bulk-mode resonators. The tested microcantilevers and square plate resonators are hard clamped to the anchors with relatively short support beams [56], [68], so clamping loss is expected to play a large role in the dissipation. The oscillation frequency varies from 100 kHz to 10 MHz for these devices, as demarcated in Table I. The resonators are individually vacuum-sealed in their own wafer-scale hermetic packaging to eliminate gas damping and surface loss [69], [70]. When the device chip containing the microcantilever is floated by wirebonds, we observe a repeatable increase in quality factor by over an order-of-magnitude relative to bonding the chip to the frame, associated with a sharp reduction in microcantilever clamping loss. By measuring the temperature-dependence of the dissipation down to cryogenic temperatures, we observe

TABLE I

Wavelength ($\lambda=2\pi v_s/\omega_0$) of Radiated Acoustic Waves as a Function of Vibration Frequency $(\omega_0/2\pi)$ for Mechanical Resonators Fabricated From Silicon [64], Silicon Nitride [65], and Lithium Niobate [66]. The Speed of Sound $(v_s=\sqrt{K/\rho})$ is Listed for Each Material and is Calculated From the Bulk Modulus (K) and Mass Density (ρ) [67]. The Range of Acoustic Wavelengths Considered in This Work is Highlighted in Green

$\omega_0/2\pi$	Single crystal silicon (6.0 km s ⁻¹)	Silicon nitride (8.7 km s ⁻¹)	Lithium niobate (4.8 km s ⁻¹)
10 kHz	600 mm	870 mm	480 mm
100 kHz	60 mm	87 mm	48 mm
1 MHz	6.0 mm	8.7 mm	4.8 mm
10 MHz	$600~\mu\mathrm{m}$	$870~\mu\mathrm{m}$	$480~\mu\mathrm{m}$
100 MHz	$60~\mu\mathrm{m}$	$87~\mu\mathrm{m}$	$48~\mu\mathrm{m}$
1 GHz	$6.0~\mu\mathrm{m}$	$8.7~\mu\mathrm{m}$	$4.8~\mu\mathrm{m}$
10 GHz	600 nm	870 nm	480 nm

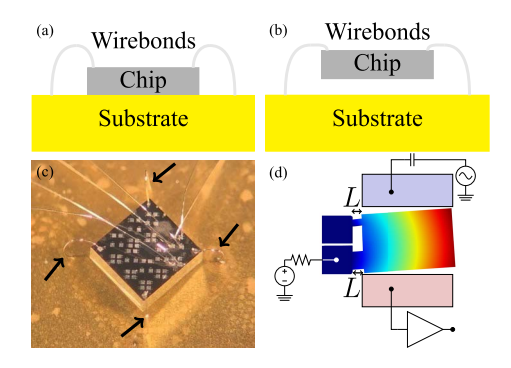


Fig. 1. (a) A chip in the "fixed" configuration. The chip is bonded to the frame, providing a large sink for acoustic radiation. (b) A chip in the "floating" configuration. The chip is suspended above the frame by wirebonds, eliminating a path for acoustic radiation. (c) An optical microscope image of an encapsulated chip in the floating configuration. The structural wirebonds are denoted with arrows. (d) The measurement schematic for the in-plane mode of the flexural devices under test. Measurement electrodes above the microcantilever (not depicted) are used to transduce the out-of-plane mode. L corresponds to the microcantilever support beam length.

clear signatures of clamping loss in the fixed chip resonators and thermoelastic dissipation in the floating chip resonators, for both the in-plane and out-of-plane flexural modes.

Figure 1(a,b) illustrates the approach used to modify the clamping loss. By suspending the chip containing the microresonator with wirebonds, the quality factor associated with the clamping loss can be tuned relative to fixing the chip to the frame. Floating the chip eliminates the major path for acoustic vibration: direct transmission from the chip into the substrate through the bonded surface under the chip. This is implemented in practice in Fig. 1(c), where wirebonds around the periphery of the chip act to simultaneously suspend and

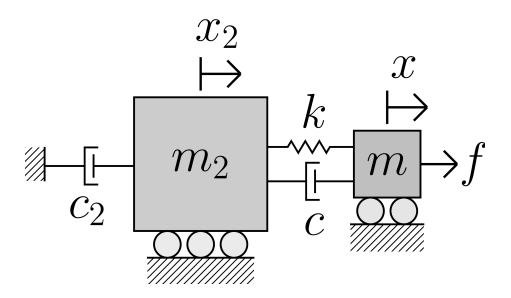


Fig. 2. A lumped model for a micro/nanoelectromechanical (MEM/NEM) vibrational mode in the presence of tunable clamping loss. x, m, k, and c are the displacement, lumped mass, stiffness, and viscous damping of the MEM/NEM mode. f is the force applied to the MEM/NEM mode. x_2 is the displacement of the chip, m_2 is the lumped mass of the chip, and c_2 accounts for the dissipation due to phonon tunneling from the chip into the frame.

stabilize the chip. Separate wirebonds connect the electrodes of the microresonator to the printed circuit board for electrical readout. The devices under test are encapsulated microcantilevers, illustrated in Fig. 1(d), and encapsulated square-plate resonators, illustrated in Fig. 8(a) and discussed in Section V.

The microcantilevers consist of a 400 μ m long, 100 μ m wide, 60 μ m thick proof mass cantilevered by a wide beam and a narrow beam. This geometry enables tuning of the effective quality factor via the thermal-piezoresistive pumping mechanism, which is not considered in this work. This geometry is interesting here because it is strongly clamping-losslimited in the fixed configuration. Clamping loss is expected to play a large role in limiting the Q in these devices because of the asymmetric anchor design. The microcantilevers are sensed capacitively via a custom low-noise transimpedance amplifier scheme [71], which enables direct measurement of the thermomechanical noise spectrum to characterize the tunable clamping loss. An optional capacitive drive is used for the cryostat experiments, to measure the quality factor via a frequency sweep across resonance or a ring-down response. Electrodes are located on either side of the microcantilever in-plane to measure the in-plane mode, and on the top surface of the encapsulation layer to measure the out-of-plane mode. No electrical current flows through the microcantilever.

III. MODEL FOR TUNABLE CLAMPING LOSS

To describe the dependence of quality factor on the chip boundary conditions, we consider the two-degree-of-freedom (2DOF) model presented in Fig. 2. To analyze this system, we apply Newton's second law to the MEM/NEM vibrational mode degree-of-freedom and chip degree-of-freedom and express the resulting system of differential equations in matrix form as:

$$\begin{bmatrix} m & 0 \\ 0 & m_2 \end{bmatrix} \begin{bmatrix} \ddot{x} \\ \ddot{x}_2 \end{bmatrix} + \begin{bmatrix} c & -c \\ -c & (c+c_2) \end{bmatrix} \begin{bmatrix} \dot{x} \\ \dot{x}_2 \end{bmatrix} + \begin{bmatrix} k & -k \\ -k & k \end{bmatrix} \begin{bmatrix} x \\ x_2 \end{bmatrix} = \begin{bmatrix} f \\ 0 \end{bmatrix}, \quad (2)$$

where m, k, and c are the lumped mass, stiffness, and viscous damping of the MEM/NEM vibrational mode, m_2 is the

chip mass, and c_2 accounts for the additional clamping loss introduced by fixing the chip to the frame.

Substituting $x(t) = X(\omega)e^{i\omega t}$, $x_2(t) = X_2(\omega)e^{i\omega t}$, and $f(t) = F(\omega)e^{i\omega t}$ into Eq. 2 and rearranging, we obtain the following matrix equation.

$$A = G^{-1}(\omega)F,\tag{3}$$

where

$$A(\omega) = \begin{bmatrix} X(\omega) \\ X_2(\omega) \end{bmatrix}, \tag{4}$$

$$F(\omega) = \begin{bmatrix} F(\omega) \\ 0 \end{bmatrix}, \tag{5}$$

$$G^{-1}(\omega) = \begin{bmatrix} G_{11}^{-1} & G_{12}^{-1} \\ G_{12}^{-1} & G_{22}^{-1} \end{bmatrix}, \tag{6}$$

and where

$$G_{11}^{-1} = \frac{1}{\omega \Delta_{+}} \left[k - m_2 \omega^2 + i \omega (c + c_2) \right],$$
 (7)

$$G_{22}^{-1} = \frac{1}{\omega \Delta_{\perp}} \left[k - m\omega^2 + i\omega c \right], \tag{8}$$

$$G_{12}^{-1} = \frac{1}{\omega \Delta_{+}} [k + i\omega c], \tag{9}$$

$$\Delta_{+} = \omega \alpha(\omega) \pm i\beta(\omega), \tag{10}$$

$$\alpha(\omega) = \omega^2 m m_2 - c c_2 - k(m + m_2), \tag{11}$$

$$\beta(\omega) = kc_2 - \omega^2 (mc + mc_2 + m_2 c). \tag{12}$$

The undamped angular resonance frequency of the MEM/NEM vibrational mode is determined from the lumped stiffness and masses of the MEM/NEM mode and chip as:

$$\omega_0 = \sqrt{\frac{k}{m} \left(1 + \frac{m}{m_2} \right)}. \tag{13}$$

A. Thermomechanical Response

The fluctuation-dissipation theorem can be employed to derive the thermomechanical displacement power-spectral-density (PSD) of the MEM/NEM mode using the real part of the admittance $Y(\omega)$ as [72]–[74]:

$$S_{xx}(\omega) = \frac{4k_B T}{\omega^2} \text{Re}\left[Y(\omega)\right]. \tag{14}$$

We define the admittance $Y(\omega)$ in terms of the relative velocity between the MEM/NEM mode and the chip as

$$Y(\omega) = \frac{V(\omega) - V_2(\omega)}{F(\omega)} = i\omega \left(G_{11}^{-1} - G_{12}^{-1} \right), \quad (15)$$

where $V(\omega)=i\omega X(\omega)$ and $V_2(\omega)=i\omega X_2(\omega)$ is the velocity of the MEM/NEM mode and chip in frequency space, respectively. This yields:

$$S_{xx}(\omega) = \frac{4k_B T \left[-c_2 \alpha(\omega) - m_2 \beta(\omega) \right]}{\Delta_+ \Delta_-},$$
 (16)

which has units of m^2 Hz^{-1} . In the measured 2DOF system, the voltage amplitude-spectral-density (ASD) at the amplifier output is thus:

$$S_{vv,2D}^{1/2}(\omega) = \sqrt{\Re^2(\omega)S_{xx}(\omega) + S_n(\omega)},$$
 (17)

which has units of V Hz^{-1/2}. \Re is the amplifier responsivity in units of V m⁻¹ and S_n is the amplifier noise spectrum in units of V² Hz⁻¹. The amplifier noise is assumed to be uncorrelated with the thermomechanical displacement fluctuations of the MEM/NEM mode, and both displacement quadratures of motion are assumed to be averaged into $S_{nv,2D}^{1/2}(\omega)$.

The thermomechanical noise ASD of the MEM/NEM mode can alternately be described by the one-degree-of-freedom (1DOF) fluctuation-dissipation model [72]. This corresponds to the limiting case of the 2DOF model for $m/m_2 = 0$. The 1DOF model is useful for defining a resonance frequency and a quality factor for comparing to the literature, and agrees well with the 2DOF model for typical values of m and m_2 . For the 1DOF system, the tunable anchor damping must be accounted for by varying the damping parameter c. The admittance of the 1DOF system is:

$$Y(\omega) = \frac{c\omega^2 + i\omega(k - m\omega^2)}{(k - m\omega^2)^2 + (c\omega)^2}.$$
 (18)

Substituting Eq. 18 into Eqs. 14 and 17, defining an angular resonance frequency $\omega_0 = \sqrt{k/m}$ and quality factor $Q = m\omega_0/c$, and simplifying yields:

$$S_{vv,1D}^{1/2}(\omega) = \sqrt{\Re^2(\omega) \frac{4k_B T \left(\frac{\omega_0}{Qm}\right)}{\left(\omega^2 - \omega_0^2\right)^2 + \left(\frac{\omega\omega_0}{Q}\right)^2} + S_n(\omega)}.$$
 (19)

B. Forced Response

The 2DOF and 1DOF models in the previous section can be adapted from the case of thermomechanical noise forcing to the case of an external forcing. Including a feedthrough signal $A_{ft}(\omega)$ between the forcing and the resonator displacement response, and a proportionality constant between amplifier output and forcing, $\mathfrak C$ in V m⁻¹, the amplitude response $A_{2D}(\omega)$ for the 2DOF model is:

$$A_{2D}(\omega) = \sqrt{\mathfrak{C}^2 |F(\omega)|^2 \frac{(\omega^2 m_2^2 + c_2^2)}{\Delta_+ \Delta_-} + A_{ft}^2(\omega)}, \quad (20)$$

and the amplitude response $A_{1D}(\omega)$ for the 1DOF model is:

$$A_{1D}(\omega) = \sqrt{\mathfrak{C}^2 |F(\omega)|^2 \frac{1/m^2}{\left(\omega^2 - \omega_0^2\right)^2 + \left(\frac{\omega\omega_0}{Q}\right)^2} + A_{ft}^2(\omega)}.$$

This model disregards the frequency-dependent phase between the resonator displacement and feedthrough signal, so is only accurate close to resonance and with low feedthrough signal.

IV. MICROCANTILEVER MEASUREMENTS

A. Thermomechanical Spectra

Figure 3(a) shows the measured room-temperature thermomechanical noise ASD of the vibrations for the in-plane mode, and Fig. 3(b) shows the thermomechanical ASD for the out-of-plane mode, of a microcantilever with a 10 μ m

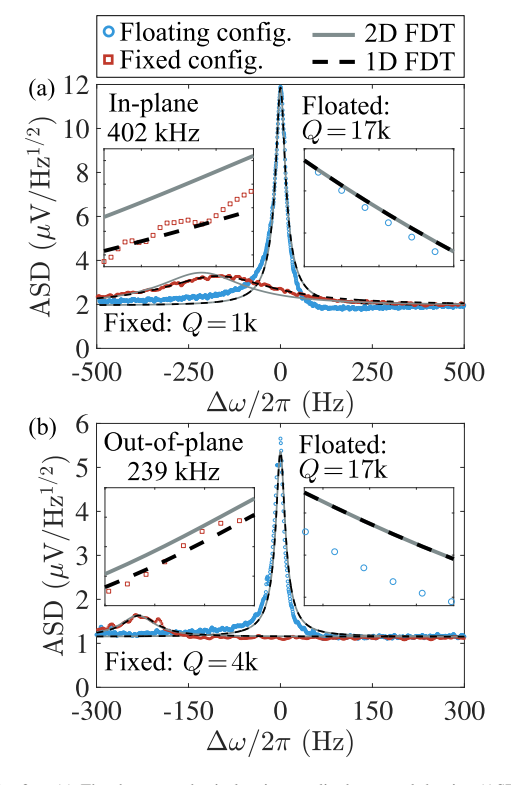


Fig. 3. (a) The thermomechanical noise amplitude-spectral-density (ASD) for the in-plane mode of the microcantilever, in the fixed (red squares) and floating (blue circles) configuration. (b) The thermomechanical noise ASD for the out-of-plane mode of the microcantilever, in the fixed (red squares) and floating (blue circles) configuration. $\Delta \omega/2\pi$ corresponds to the spectral frequency offset from resonance in the floating configuration. The ASD for the two-degree-of-freedom model (Eq. 17, gray curve) are fitted to the measured ASD to extract the parameters in Table II. For both modes, floating the chip narrows the transfer function and reduces the thermomechanical noise force. The left inset in (a) and (b) shows a zoom-in of the experimental points and model curves in the floating configuration. The right inset in (a) and (b) shows a zoom-in of the experimental points and model curves in the floating configuration, and slightly differ in the fixed configuration because the large c_2 value slightly lowers the resonance frequency. The ambient temperature is $T=298~{\rm K}$ for these measurements.

support beam length in the fixed and floating configurations. Hardened photoresist is used to fix the chip to the frame in the fixed configuration. Soaking the chip with acetone dissolves the photoresist without disturbing the wirebonds, enabling the chip to be suspended by structural wirebonds located at each corner, as depicted in Fig. 1(c). The displacement for the inplane mode is measured differentially using the electrodes on either side of the microcantilever. This eliminates the common mode noise in the amplifier and increases the signal due to the thermomechanical vibrations. The out-of-plane mode is measured using the electrodes in the top encapsulation layer above the microcantilever. The small electrode area

TABLE II EXTRACTED PARAMETERS FOR THE TWO-DEGREE-OF-FREEDOM MODEL AND THE ONE-DEGREE-OF-FREEDOM MODEL FOR THE IN-PLANE AND OUT-OF-PLANE MODES OF THE $L\!=\!10~\mu\mathrm{M}$ Microcantilever

Parameter	In- plane floated	In- plane fixed	Out- plane floated	Out- plane fixed
m [μg]	7.853	7.853	7.990	7.990
m_2 [mg]	4.660	4.660	4.660	4.660
$c \ [\mu { m g \ s^{-1}}]$	1182	1182	701.7	701.7
$c_2 \ [{ m g \ s^{-1}}]$	0	4555	0	846.8
$c_2/c \ (\times 10^3)$	0	3853.6	0	1206.8
k [kN m ⁻¹]	50.127	50.085	17.988	17.954
$\omega_0/(2\pi)$ [kHz]	402.443	402.272	239.008	238.779
Q	16765	1235	17071	3841
\mathfrak{R}_{2D} [V $\mu\mathrm{m}^{-1}$]	251.02	197.06	51.334	24.062
\mathfrak{R}_{1D} [V μ m ⁻¹]	251.02	208.97	51.334	23.996

used to sense the out-of-plane mode partly accounts for the lower amplifier responsivity compared to the in-plane mode in Table II

In order to extract the parameters for the two-degreeof-freedom and one-degree-of-freedom models in Eqs. 17 and 19, respectively, these equations are fitted to the measured thermomechanical noise ASD in Fig. 3, for both the floating and fixed configurations and both the fundamental in-plane and out-of-plane modes of the microcantilever. Because the in-plane and out-of-plane cantilever modes are well-separated in frequency space, the 2DOF and 1DOF models can be employed for each MEM/NEM mode independently [75]. For both the 2DOF and 1DOF model, the lumped modal mass m is computed using COMSOL Multiphysics. The mass of the chip m_2 is computed using a chip width, length, and thickness of 2 mm, 2 mm, and 500 μ m and a silicon density of 2330 kg m^{-3} . The viscous damping c in the 2DOF model is computed using the linewidth of the thermomechanical noise ASD in the floating configuration, setting c_2 to zero. c_2 is used to fit the 2DOF to the noise ASD in the fixed configuration, holding c constant. The lumped stiffness k in the 2DOF model is computed from the resonance frequency in the fixed and floating configurations, assuming the zero damping case $c = c_2 = 0$ kg s⁻¹ and using Eq. 13. The justification for using k as a frequency fitting parameter is that floating the chip potentially releases residual stress in the anchors. The 1DOF model is simultaneously fitted to the noise ASD to extract the associated quality factor Q and angular resonance frequency ω_0 in the floating and fixed configurations. For both the in-plane and out-of-plane modes in the floating and fixed configurations, the amplifier responsivity \Re is used as a fitting parameter.

In the floating configuration, the chip phonon tunneling parameter is set to zero ($c_2 = 0 \text{ kg s}^{-1}$), so the 2DOF model matches the 1DOF model almost exactly

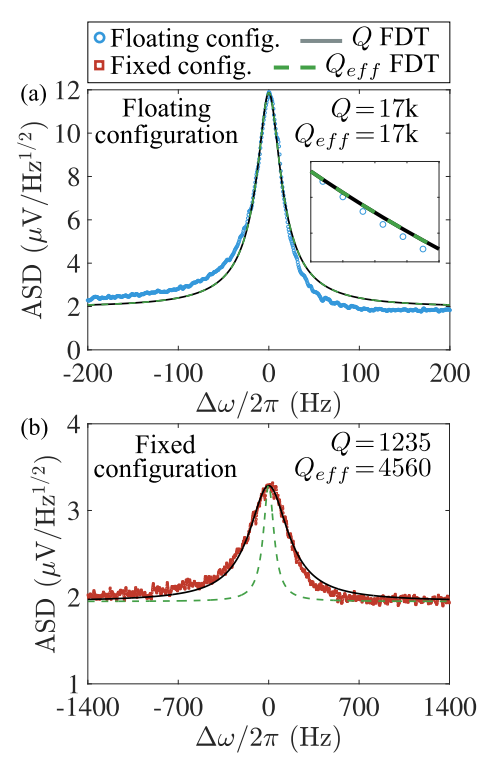


Fig. 4. (a) The thermomechanical noise amplitude-spectral-density (ASD) for the in-plane mode of the microcantilever, in the floating (blue circles) configuration. (b) The thermomechanical noise amplitude-spectral-density (ASD) for the in-plane mode of the microcantilever, in the fixed (red squares) configuration. The solid black line curve corresponds to Eq. 19 by asserting that clamping loss tunes the mechanical quality factor, and the dashed green line corresponds to an improper use of Eq. 22 by incorrectly asserting that clamping loss tunes the effective quality factor. The right inset in (a) shows a zoom-in of the experimental points and model curves in the floating configuration. The two models are identical in the floating configuration ($Q = Q_{eff}$). The dashed green curve deviates significantly from the black curve and experimental data in the fixed configuration ($Q \neq Q_{eff}$).

near the MEM/NEM mode resonance for both the in-plane and out-of-plane modes. For both the in-plane mode and out-of-plane mode in the fixed configuration, the fitted 2DOF model has a slight frequency detuning relative to the measured ASD and the 1DOF model. This is attributed to a shift in the damped resonance frequency away from the undamped resonance frequency in Eq. 13 at the large c_2 value required to fit the 2DOF model to the measured thermomechanical ASD in the fixed configuration. Because the increase in clamping loss in the fixed configuration is more pronounced for the in-plane mode than the out-of-plane mode, the damping-induced shift in resonance frequency is larger for the in-plane mode than the out-of-plane mode.

Clamping loss tunes the mechanical quality factor in Eq. 1, not the effective quality factor like thermal-piezoresistive pumping and the other effective quality factor tuning mechanisms [3]. We can confirm this experimentally using the

measured thermomechanical ASD and Eq. 19. Tuning the mechanical quality factor with variable clamping loss modifies both the resonator transfer function in the denominator and the thermomechanical noise force PSD in the numerator of Eq. 19. The PSD of the thermomechanical noise forcing applied to the MEM/NEM mode is accounted for by the \mathcal{Q} in the numerator of Eq. 19.

The measured thermomechanical noise spectrum for effective quality factor tuning is given by:

$$S_{vv,Q_{eff}}^{1/2}(\omega) = \sqrt{\Re^2(\omega) \frac{4k_B T \left(\frac{\omega_0}{Qm}\right)}{\left(\omega^2 - \omega_0^2\right)^2 + \left(\frac{\omega\omega_0}{Q_{eff}}\right)^2} + S_n(\omega)}, \quad (22)$$

Equation 22 differs from Eq. 19 because effective quality factor tuning does not modify the thermomechanical noise force PSD.

Figure 4 shows the measured thermomechanical ASD for the in-plane mode of the microcantilever in the floating and fixed configurations, along with Eqs. 19 and 22. Fixing the chip to the substrate causes the linewidth to increase and the noise force to increase, consistent with an increase in mechanical quality factor associated with increasing clamping loss. This is properly accounted for by decreasing Q in Eq. 19. Incorrectly attempting to fit Eq. 22 to the noise ASD by assuming that variable clamping loss only varies the effective quality factor results in a peak that is too narrow compared to the measured thermomechanical ASD in the fixed configuration. Variable clamping loss thus modifies the mechanical, not effective, quality factor. This result is similar to the recent experiments by Bousse et al., which showed that electrical damping due to dissipation across a capacitively coupled resistor reduces the mechanical quality factor, not the effective quality factor [76].

B. Dependence on Support Beam Length

Figure 5 shows measurements of the quality factor and resonance frequency for the in-plane mode and out-of-plane mode for a set of microcantilevers with varying support beam length from $L\!=\!10~\mu\mathrm{m}$ to $L\!=\!100~\mu\mathrm{m}$, in both the fixed and floating configuration. The thermomechanical noise spectra are measured for both modes at a microcantilever bias voltage of 120 V with respect to the adjacent sense electrodes.

The substantial increase in quality factor in the floating configuration compared to the fixed configuration is demonstrated in Fig. 5(a), and is consistent for both the in-plane and out-of-plane modes, for all of the measured microcantilevers. For a given type of boundary condition, there is significant variability in the measured quality factor between the in-plane and out-of-plane modes, and variability with varying support beam length. In the fixed configuration, the quality factor increases slightly as the beam length is increased, which can be explained by the decreasing stress gradients near the attachment points of the support beams with the anchors for the longer beams. Simulations of the quality factor arising from thermoelastic dissipation are performed using COMSOL, and show that the quality factor is TED-limited for both modes

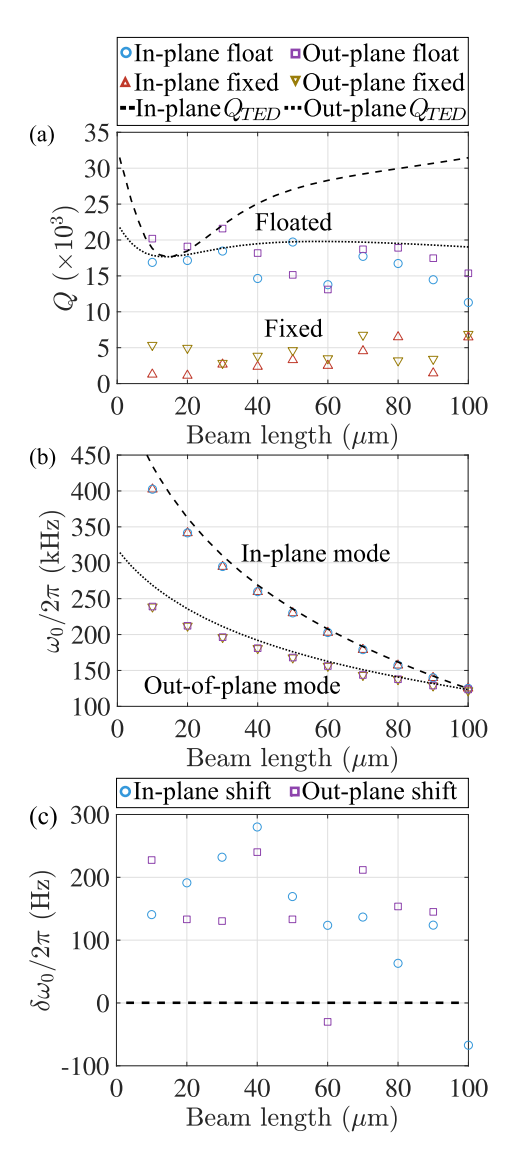


Fig. 5. (a) The measured quality factor of the in-plane mode in the fixed (upward red triangles) configuration and the floating (blue circles) configuration, and the out-of-plane mode in the fixed (downward yellow triangles) and floating (purple squares) configuration. The simulated Q due to thermoelastic dissipation is overlaid for the in-plane mode (dashed black curve) and the out-of-plane mode (dotted black curve). (b) The measured resonance frequency of the in-plane and out-of-plane mode in the fixed and floating configuration. The simulated eigenfrequencies as a function of support beam length are overlaid for the in-plane mode (dashed black curve) and out-of-plane mode (dotted black curve). The plot markers follow the same convention as in (a). (c) The measured frequency difference $\delta\omega_0/2\pi = (\omega_0,floated-\omega_0,fixed)/2\pi$ for the in-plane mode (blue circles) and out-of-plane mode (purple squares). The thick dashed black line demarcates a positive and negative frequency difference.

of the floated microcantilevers with short support beams, but remains slightly clamping-loss-limited for the in-plane mode as the beam length is increased. The variability in quality

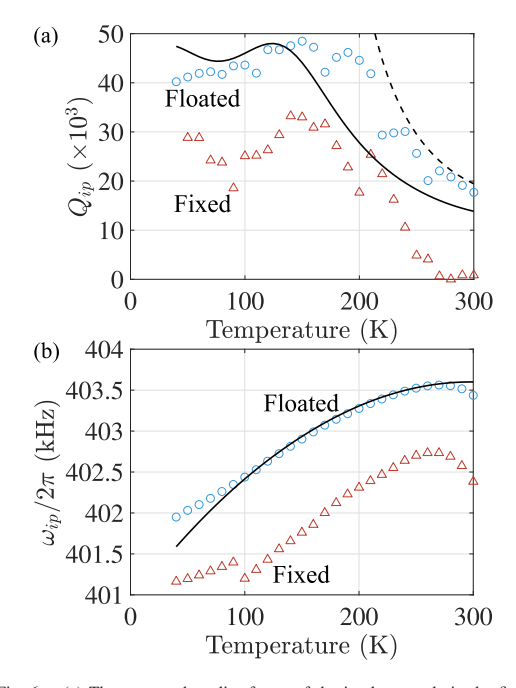


Fig. 6. (a) The measured quality factor of the in-plane mode in the fixed (upward red triangles) and floating (blue circles) configuration. The simulated quality factor curves corresponding to thermoelastic dissipation (TED) only (dashed black curve) and combined TED with constant clamping loss $Q_{clamp} = 48$ k (solid black curve) are overlaid. (b) The measured resonance frequency of the in-plane mode in the fixed (upward red triangles) and floating (blue circles) configuration. The simulated resonance frequency (black curve) is overlaid.

factor in the floating long support beam resonators could be due to the remaining clamping loss, which in turn depends on the residual stress in the anchors and the several encapsulation layers in the chip.

The measured resonance frequency for the microcantilever modes are plotted as a function of support beam length in Fig. 5(b), and the corresponding simulated eigenfrequency curves are overlaid. The eigenfrequency simulations include 250 nm of over-etch in the support beams and proof mass relative to the nominal dimensions [71], and electrostatic softening to the adjacent side and top electrodes with a device bias voltage of 120 V, an in-plane electrode gap of 850 nm, and an out-of-plane gap of 2.5 μ m.

The resonance frequency difference for a given microcantilever mode between the floating and fixed configuration is plotted as a function of beam length in Fig. 5(c). After floating a chip, the resonance frequency shifts upward by roughly 100 Hz to 300 Hz for both modes fairly consistently. The frequency upshift with floating does not exhibit any clear dependence on support beam length.

C. Temperature Study

Figures 6 and 7 present measurements of the quality factor and resonance frequency for the in-plane and out-of-plane

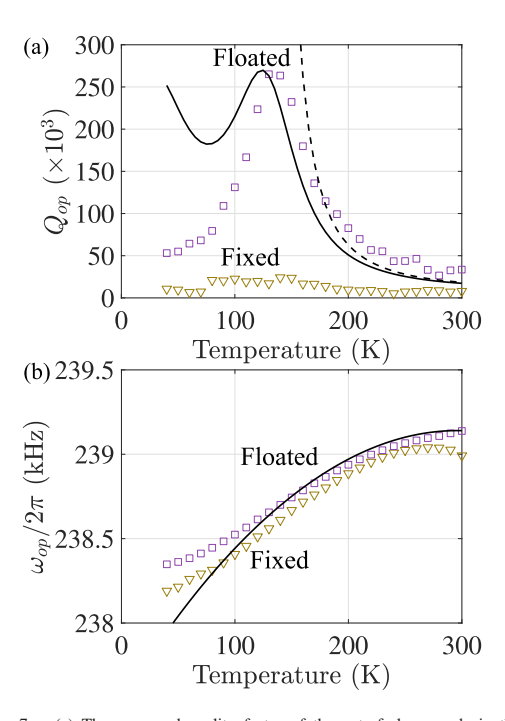


Fig. 7. (a) The measured quality factor of the out-of-plane mode in the fixed (downward yellow triangles) and floating (purple squares) configuration. The simulated quality factor curves corresponding to thermoelastic dissipation (TED) only (dashed black curve) and combined TED with constant clamping loss $Q_{clamp} = 270 \mathrm{k}$ (solid black curve) are overlaid. (b) The measured resonance frequency of the out-of-plane mode in the fixed (downward yellow triangles) and floating (purple squares) configuration. The simulated resonance frequency (black curve) is overlaid.

modes of a microcantilever with a support beam length of $L=10~\mu \mathrm{m}$. The temperature measurements are performed in a closed-cycle helium cryostat, for temperatures ranging from 40 K to 300 K. A low-noise cryostat feedthrough enables the use of the capacitive readout to detect the vibrations of the in-plane and out-of-plane modes. At each cryostat temperature, the resonance frequency is extracted using the peak center in the directly driven response, and the quality factor is extracted by fitting a decaying exponential function to the ring-down response.

COMSOL simulations of the temperature-dependent thermoelastic dissipation and resonance frequencies were additionally performed to estimate Q_{TED} and $\omega_0/2\pi$ for the in-plane and out-of-plane modes. The anisotropic silicon model was employed with a temperature-dependent coefficient of thermal expansion and set of elastic moduli. The temperature-dependent coefficient of thermal expansion used in the simulations was reported by Middelmann *et al.* [77]. Temperature-dependent elastic moduli up to second-order in temperature, as measured by Ng *et al.* for a phosphorus doping concentration of 6.6×10^{19} cm⁻³, were used [78]. The total quality factor is estimated by assuming that only clamping loss and TED contribute to Eq. 1, and that

clamping loss is constant with temperature. The simulated resonance frequency curves are shifted to overlay on top of the measured resonance frequencies, to account for the static shift in resonance frequency arising from electrostatic softening and over-etch of the geometry.

The measured resonance frequency decreases with decreasing temperature for both the in-plane mode and out-of-plane mode, and yield a good agreement with the simulated resonance frequency down to 100 K. At this temperature, thirdorder doping-dependent temperature coefficients of elasticity would be necessary to yield a good agreement between the measurements and simulations. In the fixed configuration for both modes, and also the floating configuration for the in-plane mode, the room-temperature resonance frequency actually increases with decreasing temperature, in disagreement with the simulated frequency dependence based on temperaturedependent elasticity. This negative temperature-coefficient-offrequency (TCF) near room-temperature most likely arises from the residual stress in the anchors. Floating the chip releases some of the residual stress, reducing the magnitude of the negative TCF for the in-plane mode and reversing the sign of the TCF for the out-of-plane mode. The much larger measured quality factors in the floated out-of-plane mode compared to the floated in-plane mode at 125 K suggests some relationship between the trapped residual stress in the anchors and the tunable clamping loss.

For both the in-plane mode and out-of-plane mode, clamping loss limits the quality factor over all temperatures in the fixed configuration. In the floating configuration, the quality factor is limited by TED from room temperature down to 200 K for the in-plane mode and 150 K for the out-of-plane mode. Below these temperatures, the clamping loss is once more the limiting dissipation mechanism in the floating configuration. Assuming a constant clamping loss, $Q_{clamp} \approx 48 \mathrm{k}$ for the in-plane mode and $Q_{clamp} \approx 270 \mathrm{k}$ for the out-of-plane mode. In both modes, a decrease in Qclamp with decreasing temperature below 100 K appears to be necessary to track the drop in quality factor at low temperatures, suggesting that clamping loss does not remain constant in the microcantilevers over varying temperature. Another possibility is that a different damping mechanism is becoming prominent below 100 K, but at least to the author's knowledge, the other possibilities, such as increasing gas damping, surface loss, Akhiezer dissipation, electrical damping, or dissipation due to two-level defects are not likely. The quality factor due to gas damping is known to increase with decreasing temperature [79]. Surface loss is believed to be negligible for these devices because of the hermetic vacuum encapsulation, as well as the relatively low surfaceto-volume ratio compared to the nanomechanical resonators for which surface loss is prominent [80]. Akhiezer-limited Q is routinely reached in silicon encapsulated bulk-mode micromechanical resonators that attain resonance-frequencyquality-factor products $>10^{13}$ [32], [81], [82]. The measured products in Figs. 6 and 7 are several orders of magnitude below this limit, so Akhiezer dissipation is not expected to play a role. Slight electrical damping occurs in the first stage feedback resistor of the thermomechanical-noise-limited amplifier above 140 V bias for the microcantilever geometry, however the operating voltage is well below 140 V, a low gain amplifier is used for the cryostat experiment, and the amplifier is located outside of the cryostat and remains at room temperature. Recent measurements in silicon nanomechanical resonators suggest that the dissipation due to two-level defects may become observable below 10 K for mechanical quality factors in excess of $\approx 10^9$ [51], [83], however the measured quality factors in Figs. 6 and 7 are more than 4 orders of magnitude lower than those measurements and are at substantially higher temperatures. One plausible explanation for the temperature-dependent Q_{clamp} is that the differential expansion of the various layers in the resonator encapsulation modifies the interfacial impedance at the resonator anchors through varying stress, which imparts a temperature dependence to the clamping loss and resonance frequency.

V. BULK-MODE RESONATOR MEASUREMENTS

In this section, we demonstrate tunable clamping loss in a bulk-mode resonator, and fit the model for tunable clamping loss to extract the parameters in the model presented in Section III. The measured square plate resonator has a length and width of 400 μ m, and a thickness of 42.5 μ m. The square plate has an adjacent electrode on each side for transduction of the Lamé mode at a resonance frequency of approximately 10 MHz. The device is anchored at each corner, corresponding to nodes in the Lamé mode shape, by 3.5 μ m wide by 8.2 μm long beams. Fig. 8(a) illustrates the Lamé mode shape and electrical setup. Because the opposite sides are in-phase for the Lamé mode shape, the transduction setup capacitively drives one pair of electrodes with a harmonic voltage and capacitively senses the resulting motional current through the other pair of electrodes via a transimpedance amplifier. At 10 MHz frequencies, the signal-to-noise ratio of the capacitive readout is not large enough to detect the thermomechanical fluctuations of the Lamé mode, so the driven response is employed to measure the quality factor and resonance frequency.

This square plate resonator is limited by clamping loss, as was previously determined through measurements of quality factor for this geometry over the temperature range from 110 K to 300 K [32]. Separate finite element simulations predict Q_{TED} to be greater than 10^8 . The Akhiezer limit for the Lamé mode at $\omega_0/2\pi=10.07$ MHz is $Q_{phon}=2.6$ M. This device was tested at room temperature in both the fixed and floating configurations, yielding measured quality factor values of 317k and 1.35M, respectively. In agreement with the flexural mode resonator tested in Section IV, by removing the direct acoustic radiation sink arising in the bonded chip configuration, the clamping loss is reduced.

In a similar procedure to fitting the 1DOF and 2DOF models to the microcantilever thermomechanical response, the forced response 1DOF and 2DOF models (Eqs. 20 and 21) from Section III.B are fitted to the driven response of the Lamé mode of the square plate resonator. The 2DOF model, in grey, is fitted to the driven responses in the fixed and floating configurations in Fig. 8(b). The 1DOF model, in dashed black,

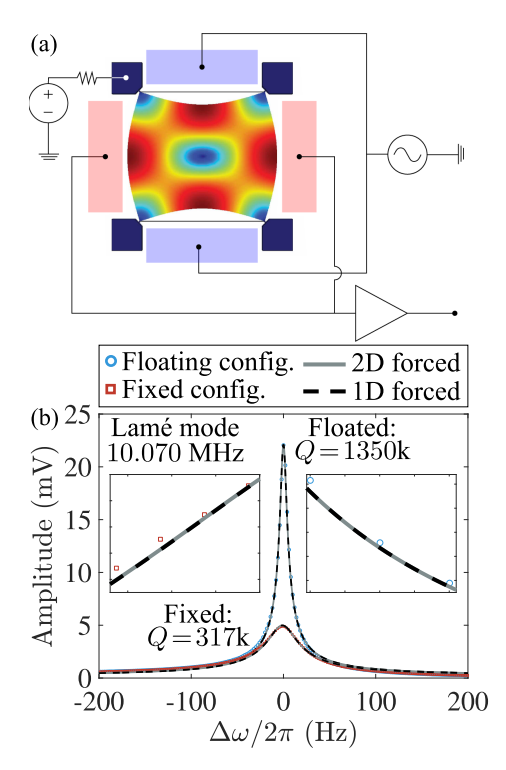


Fig. 8. (a) The measurement schematic for the Lamé mode of the square plate resonator. The resonator is biased at 120 V with respect to the electrodes, and is driven using two opposing electrodes (in blue) and sensed with the complementary two opposing electrodes (in red). (b) The driven response for the Lamé mode of a square plate resonator in the floated and fixed configurations, with the forced responses in Eqs. 20 (gray curve) and 21 (dashed black curve) overlaid. The left inset shows a zoom-in of the experimental points and model curves in the fixed configuration. The right inset shows a zoom-in of the experimental points and model curves in the floating configuration. The ambient temperature is $T=298~{\rm K}$ for these measurements.

is fitted to the driven responses in the fixed and floating configurations. In the fixed case, c_2 for the Lamé mode increases to 444.5 mg s⁻¹.

Because the resonance frequency and quality factor of the Lamé mode is nearly two orders of magnitude larger than the microcantilever fundamental flexural modes, c for the Lamé mode of the square plate resonator is about three orders of magnitude lower than both modes of the microcantilever to yield a similar linewidth for all three modes in the floating configuration. The impact of fixing the chip to the substrate on the damping can be compared for the flexural modes and bulk mode via the ratio c_2/c ; a larger ratio corresponds to a relatively larger impact of the modified chip boundary conditions on the clamping loss. $c_2/c = 1267 \times 10^3$ for the Lamé mode, $c_2/c = 1207 \times 10^3$ for the out-of-plane microcantilever mode, and $c_2/c = 3854 \times 10^3$ for the in-plane microcantilever mode. The c_2/c ratio for the Lamé mode and out-of-plane microcantilever mode differ by less than 5%,

TABLE III

EXTRACTED PARAMETERS FOR THE TWO-DEGREE-OF-FREEDOM MODEL
AND THE ONE-DEGREE-OF-FREEDOM MODEL FOR THE LAMÉ MODE
OF THE SOUARE PLATE RESONATOR

Parameter	Lamé floated	Lamé fixed	
$m [\mu g]$	7.486	7.486	
m_2 [mg]	4.660	4.660	
$c [\operatorname{ng} \operatorname{s}^{-1}]$	350.8	350.8	
$c_2 \ [{\rm mg \ s^{-1}}]$	0	444.5	
$c_2/c \; (\times 10^3)$	0	1267.1	
k [MN m ⁻¹]	29.91967	29.91966	
$\omega_0/(2\pi)$ [MHz]	10.069831	10.069830	
$Q (\times 10^3)$	1347	317	
$\mathfrak{C}_{2D}F \text{ [mN V m}^{-1}\text{]}$	492	492	
$\mathfrak{C}_{1D}F \text{ [mN V m}^{-1}\text{]}$	471	471	

while c_2/c for the in-plane microcantilever mode is three times larger than for the other modes. The larger c_2/c ratio, along with the lower quality factor near 125 K in Fig. 6(a) and the negative TCF near room temperature in Fig. 6(b) in the floating configuration, suggests that clamping loss plays the largest role in the in-plane microcantilever mode. This could be because the asymmetric support beams result in the largest shear and bending stress in the anchors for the in-plane mode during vibrations, and make the clamping loss for this mode particularly sensitive to residual stress in the encapsulation layers.

These measurements make it clear that boundary conditions far away from the vibrating structure can have a large impact on dissipation in a wide variety of radiofrequency micromechanical resonators. We also note that the tunable clamping loss for the microcantilevers and Lamé mode resonators with varying chip boundary conditions does not depend on the method used to measure quality factor; separate ring-down measurements on these devices corroborate the quality factor values presented in Tables II and III. If clamping loss is a limiting dissipation mechanism in a MEM/NEM resonator. modifying the boundary conditions of the chip with the frame can substantially improve the post-fabrication Q. For many applications, clamping loss can be minimized at the anchors through symmetric anchors [18], compliant tethers [26], [29], [32], or soft-clamping [41], [43]. For the resonator designs that are often limited by clamping loss, modifying the chip boundary conditions as is demonstrated in this work can be used to improve Q.

Recent measurements show that the choice of mounting adhesive between the chip and frame can alter the clamping loss [56]. This suggests that a mounting adhesive could be developed which dramatically alters the interfacial impedance between the chip and the frame in response to an applied stimulus, such as an applied electric or magnetic field, which could modify the clamping loss of the on-chip resonators. Such an adhesive could enable in-situ tuning of the clamping

loss in MEM/NEM resonators without the difficulty of floating the chip or the fragility of the wirebond suspension. Another approach for in-situ tuning of clamping loss is the precise positioning of an atomic force microscope tip at the anchors to modify the mechanical impedance mismatch of the resonator with the environment [58]. At present, perhaps the easiest strategy for in-situ tuning of the mechanical quality factor across a variety of MEM/NEM resonators is electrical damping, which only requires a static voltage to control the vibration-induced dissipative current through the resonator or an external resistor [76], [84], [85]. For force sensing measurements, high Q is desirable for a high signal-to-noise ratio while the resonator transients can be damped out via Q_{eff} suppression without increasing the thermomechanical noise force [3], [86], [87]. So for sensing applications limited by the resonator thermomechanical vibrations, the Q_{eff} tuning mechanisms should be utilized in lieu of mechanical Q tuning such as clamping loss to avoid degrading the SNR.

VI. CONCLUSION

In this Article, we demonstrate tunable clamping loss in encapsulated micromechanical resonators, by adjusting the boundary conditions of the chip with the frame. We propose and experimentally confirm a two-degree-of-freedom model to describe this effect via an additional viscous dissipation channel through the frame. By comparing the measured thermomechanical noise to the fluctuation-dissipation theorem, we show that the variable clamping loss in these devices modifies the mechanical, not effective, quality factor. We show that varying the chip boundary conditions can tune the quality factor of a flexural-mode resonator by more than an order of magnitude, and the quality factor of a bulk-mode resonator by more than a factor of three. This work shows that for radiofrequency micromechanical resonators, boundary conditions far away from the actual vibrating elements can have a large impact on the clamping loss, and that clamping loss may exhibit temperature-dependence via stress-induced mechanical impedance mismatching.

ACKNOWLEDGMENT

James M. L. Miller is grateful for the helpful discussions with Amir Safavi-Naeini, Donghao Li, Nicholas Bousse, Haoshen Zhu, and Yupeng Tian. The authors are grateful to Dusan Coso and Seid Sadat for their early work on the helium cryostat setup. Fabrication was performed at the nano@Stanford Labs. The data that support the findings of this study are available from the corresponding authors upon reasonable request.

REFERENCES

- R. Bogue, "MEMS sensors: Past, present and future," Sensor Rev., vol. 27, no. 1, pp. 7–13, Jan. 2007.
- [2] S. Zaliasl et al., "A 3 ppm 1.5×0.8 mm² 1.0 μA 32.768 kHz MEMS-based oscillator," IEEE J. Solid-State Circuits, vol. 50, no. 1, pp. 291–302, Jan. 2015.
- [3] J. M. L. Miller et al., "Effective quality factor tuning mechanisms in micromechanical resonators," Appl. Phys. Rev., vol. 5, no. 4, Dec. 2018, Art. no. 041307.

- [4] D. Kleckner and D. Bouwmeester, "Sub-kelvin optical cooling of a micromechanical resonator," *Nature*, vol. 444, no. 7115, pp. 75–78, Nov. 2006.
- [5] J. D. Teufel et al., "Sideband cooling of micromechanical motion to the quantum ground state," *Nature*, vol. 475, no. 7356, pp. 359–363, Jul. 2011.
- [6] P. G. Steeneken et al., "Piezoresistive heat engine and refrigerator," Nature Phys., vol. 7, no. 4, pp. 354–359, Apr. 2011.
- [7] G. Bahl, M. Tomes, F. Marquardt, and T. Carmon, "Observation of spontaneous Brillouin cooling," *Nature Phys.*, vol. 8, no. 3, pp. 203–207, Mar. 2012
- [8] C. Urgell et al., "Cooling and self-oscillation in a nanotube electromechanical resonator," Nature Phys., vol. 16, no. 1, pp. 32–37, Jan. 2020.
- [9] C. T.-C. Nguyen and R. T. Howe, "An integrated CMOS micromechanical resonator high-Q oscillator," *IEEE J. Solid-State Circuits*, vol. 34, no. 4, pp. 440–455, Apr. 1999.
- [10] X. L. Feng, C. J. White, A. Hajimiri, and M. L. Roukes, "A self-sustaining ultrahigh-frequency nanoelectromechanical oscillator," *Nature Nanotechnol.*, vol. 3, no. 6, pp. 342–346, 2008.
- Nanotechnol., vol. 3, no. 6, pp. 342–346, 2008.
 [11] G. Bahl, J. Zehnpfennig, M. Tomes, and T. Carmon, "Stimulated optomechanical excitation of surface acoustic waves in a microdevice," Nature Commun., vol. 2, no. 1, pp. 1–6, Sep. 2011.
- [12] M. Serra-Garcia, A. Foehr, M. Molerón, J. Lydon, C. Chong, and C. Daraio, "Mechanical autonomous stochastic heat engine," *Phys. Rev. Lett.*, vol. 117, no. 1, Jun. 2016, Art. no. 010602.
- [13] J. F. Rhoads, S. W. Shaw, and K. L. Turner, "Nonlinear dynamics and its applications in micro- and nanoresonators," *J. Dyn. Syst., Meas., Control*, vol. 132, no. 3, pp. 034001-1–034001-14, May 2010.
- [14] C. Chen, D. H. Zanette, J. R. Guest, D. A. Czaplewski, and D. López, "Self-sustained micromechanical oscillator with linear feedback," *Phys. Rev. Lett.*, vol. 117, no. 1, Jul. 2016, Art. no. 017203.
- [15] S. Tiwari and R. N. Candler, "Using flexural MEMS to study and exploit nonlinearities: A review," J. Micromech. Microeng., vol. 29, no. 8, Aug. 2019, Art. no. 083002.
- [16] O. Shoshani and S. W. Shaw, "Resonant modal interactions in micro/nano-mechanical structures," *Nonlinear Dyn.*, vol. 104, pp. 1–28, Apr. 2021.
- [17] J. M. L. Miller, A. Gomez-Franco, D. D. Shin, H.-K. Kwon, and T. W. Kenny, "Amplitude stabilization of micromechanical oscillators using engineered nonlinearity," *Phys. Rev. Res.*, vol. 3, no. 3, Sep. 2021, Art. no. 033268.
- [18] R. Zhang et al., "Integrated tuning fork nanocavity optomechanical transducers with high $f_M \, Q_M$ product and stress-engineered frequency tuning," Appl. Phys. Lett., vol. 107, no. 13, Sep. 2015, Art. no. 131110.
- [19] K. Wang, A.-C. Wong, and C. T.-C. Nguyen, "VHF free-free beam high-Q micromechanical resonators," *J. Microelectromech. Syst.*, vol. 9, no. 3, pp. 347–360, Sep. 2000.
- [20] X. M. H. Huang, X. L. Feng, C. A. Zorman, M. Mehregany, and M. L. Roukes, "VHF, UHF and microwave frequency nanomechanical resonators," *New J. Phys.*, vol. 7, no. 1, p. 247, 2005.
- [21] Y.-W. Lin, L.-W. Hung, S.-S. Li, Z. Ren, and C. T.-C. Nguyen, "Quality factor boosting via mechanically-coupled arraying," in *Proc. IEEE Transducers*, Jun. 2007, pp. 2453–2456.
- [22] G. Anetsberger, R. Rivière, A. Schliesser, O. Arcizet, and T. J. Kippenberg, "Ultralow-dissipation optomechanical resonators on a chip," *Nature Photon.*, vol. 2, no. 10, pp. 627–633, Oct. 2008.
- [23] S. Wang et al., "Nonlinearity of hermetically encapsulated high-Q double balanced breathe-mode ring resonator," in Proc. IEEE 23rd Int. Conf. Microelectromech. Syst. (MEMS), Jan. 2010, pp. 715–718.
- [24] B. P. Harrington and R. Abdolvand, "In-plane acoustic reflectors for reducing effective anchor loss in lateral–extensional MEMS resonators," *J. Micromech. Microeng.*, vol. 21, no. 8, Jul. 2011, Art. no. 085021.
- [25] G. D. Cole, I. Wilson-Rae, K. Werbach, M. R. Vanner, and M. Aspelmeyer, "Phonon-tunnelling dissipation in mechanical resonators," *Nature Commun.*, vol. 2, no. 1, pp. 1–8, Sep. 2011.
- [26] J. E.-Y. Lee, J. Yan, and A. A. Seshia., "Study of lateral mode SOI-MEMS resonators for reduced anchor loss," J. Micromech. Microeng., vol. 21, no. 4, 2011, Art. no. 045010.
- [27] Y. Yang, E. J. Ng, C. H. Ahn, V. A. Hong, E. Ahadi, and T. W. Kenny, "Mechanical coupling of dual breathe-mode ring resonator," in *Proc. Transducers Eurosensors*, Jun. 2013, pp. 502–505.

- [28] J. Segovia-Fernandez, M. Cremonesi, C. Cassella, A. Frangi, and G. Piazza, "Anchor losses in AlN contour mode resonators," *J. Micro-electromech. Syst.*, vol. 24, no. 2, pp. 265–275, Apr. 2015.
- [29] D. D. Gerrard, E. J. Ng, C. H. Ahn, V. A. Hong, Y. Yang, and T. W. Kenny, "Modeling the effect of anchor geometry on the quality factor of bulk mode resonators," in *Proc. Transducers*, Jun. 2015, pp. 1997–2000.
- [30] J. Zou, C.-M. Lin, and A. P. Pisano, "Anchor loss suppression using butterfly-shaped plates for AIN Lamb wave resonators," in *Proc. Joint Conf. IEEE Int. Freq. Control Symp. Eur. Freq. Time Forum*, Apr. 2015, pp. 432–435.
- [31] B. Gibson, K. Qalandar, C. Cassella, G. Piazza, and K. L. Foster, "A study on the effects of release area on the quality factor of contourmode resonators by laser Doppler vibrometry," *IEEE Trans. Ultrason.*, *Ferroelectr., Freq. Control*, vol. 64, no. 5, pp. 898–904, May 2017.
- [32] G. D. Vukasin et al., "Anchor design affects dominant energy loss mechanism in a Lamé mode MEM resonator," J. Microelectromech. Syst., vol. 29, no. 5, pp. 860–866, Oct. 2020.
- [33] M. Eichenfield, J. Chan, R. M. Camacho, K. J. Vahala, and O. Painter, "Optomechanical crystals," *Nature*, vol. 462, pp. 78–82, Nov. 2009.
- [34] J. Chan, A. H. Safavi-Naeini, J. T. Hill, S. Meenehan, and O. Painter, "Optimized optomechanical crystal cavity with acoustic radiation shield," Appl. Phys. Lett., vol. 101, no. 8, Aug. 2012, Art. no. 081115.
- [35] A. H. Safavi-Naeini, J. T. Hill, S. Meenehan, J. Chan, S. Gröblacher, and O. Painter, "Two-dimensional phononic-photonic band gap optomechanical crystal cavity," *Phys. Rev. Lett.*, vol. 112, no. 15, Apr. 2014, Art. no. 153603.
- [36] J. Gomis-Bresco et al., "A one-dimensional optomechanical crystal with a complete phononic band gap," *Nature Commun.*, vol. 5, no. 1, pp. 1–6, Dec. 2014.
- [37] P.-L. Yu et al., "A phononic bandgap shield for high-Q membrane microresonators," Appl. Phys. Lett., vol. 104, no. 2, Jan. 2014, Art. no. 023510.
- [38] D. Feng, D. Xu, G. Wu, B. Xiong, and Y. Wang, "Phononic crystal strip based anchors for reducing anchor loss of micromechanical resonators," *J. Appl. Phys.*, vol. 115, no. 2, Jan. 2014, Art. no. 024503.
- [39] H. Zhu and J. E. Lee, "Design of phononic crystal tethers for frequency-selective quality factor enhancement in AlN piezoelectric-on-silicon resonators," *Proc. Eng.*, vol. 120, pp. 516–519, Jan. 2015.
- [40] P. Qin, H. Zhu, J. E.-Y. Lee, and Q. Xue, "Phase noise reduction in a VHF MEMS-CMOS oscillator using phononic crystals," *IEEE J. Electron Devices Soc.*, vol. 4, no. 3, pp. 149–154, May 2016.
- [41] Y. Tsaturyan, A. Barg, E. S. Polzik, and A. Schliesser, "Ultracoherent nanomechanical resonators via soft clamping and dissipation dilution," *Nature Nanotechnol.*, vol. 12, pp. 776–783, Jun. 2017.
- [42] V. J. Gokhale and J. J. Gorman, "Approaching the intrinsic quality factor limit for micromechanical bulk acoustic resonators using phononic crystal tethers," Appl. Phys. Lett., vol. 111, no. 1, 2017, Art. no. 013501.
- [43] A. H. Ghadimi, D. J. Wilson, and T. J. Kippenberg, "Radiation and internal loss engineering of high-stress silicon nitride nanobeams," *Nano Lett.*, vol. 17, no. 6, pp. 3501–3505, Jun. 2017.
- [44] R. N. Patel, C. J. Sarabalis, W. Jiang, J. T. Hill, and A. H. Safavi-Naeini, "Engineering phonon leakage in nanomechanical resonators," *Phys. Rev. Appl.*, vol. 8, no. 4, Oct. 2017, Art. no. 041001.
- [45] A. H. Ghadimi et al., "Elastic strain engineering for ultralow mechanical dissipation," Science, vol. 360, pp. 764–768, May 2018.
- [46] R. N. Patel, Z. Wang, W. Jiang, C. J. Sarabalis, J. T. Hill, and A. H. Safavi-Naeini, "Single-mode phononic wire," *Phys. Rev. Lett.*, vol. 121, no. 4, Jul. 2018, Art. no. 040501.
- [47] P. Kharel, Y. Chu, M. Power, W. H. Renninger, R. J. Schoelkopf, and P. T. Rakich, "Ultra-high-Q phononic resonators on-chip at cryogenic temperatures," APL Photon., vol. 3, no. 6, 2018, Art. no. 066101.
- [48] P. Arrangoiz-Arriola, E. A. Wollack, M. Pechal, J. D. Witmer, J. T. Hill, and A. H. Safavi-Naeini, "Coupling a superconducting quantum circuit to a phononic crystal defect cavity," *Phys. Rev. X*, vol. 8, no. 3, Jul. 2018, Art. no. 031007.
- [49] M. Kalaee, M. Mirhosseini, P. B. Dieterle, M. Peruzzo, J. M. Fink, and O. Painter, "Quantum electromechanics of a hypersonic crystal," *Nature Nanotechnol.*, vol. 14, no. 4, pp. 334–339, Apr. 2019.
- [50] A. H. Safavi-Naeini, D. Van Thourhout, R. Baets, and R. Van Laer, "Controlling phonons and photons at the wavelength scale: Integrated photonics meets integrated phononics," *Optica*, vol. 6, no. 2, pp. 213–232, 2019.

- [51] G. S. MacCabe et al., "Nano-acoustic resonator with ultralong phonon lifetime," Science, vol. 370, no. 6518, pp. 840–843, Nov. 2020.
- [52] W. Jiang et al., "Efficient bidirectional piezo-optomechanical transduction between microwave and optical frequency," Nature Commun., vol. 11, no. 1, pp. 1–7, 2020.
- [53] L. Catalini, M. Rossi, E. C. Langman, and A. Schliesser, "Modeling and observation of nonlinear damping in dissipation-diluted nanomechanical resonators," *Phys. Rev. Lett.*, vol. 126, no. 17, Apr. 2021, Art. no. 174101.
- [54] D. J. Wilson, C. A. Regal, S. B. Papp, and H. Kimble, "Cavity optomechanics with stoichiometric SiN films," *Phys. Rev. Lett.*, vol. 103, no. 20, 2009, Art. no. 207204.
- [55] T. P. Purdy, R. W. Peterson, P. L. Yu, and C. A. Regal, "Cavity optomechanics with Si₃N₄ membranes at cryogenic temperatures," *New J. Phys.*, vol. 14, no. 11, 2012, Art. no. 115021.
- [56] J. Rodriguez et al., "Direct detection of anchor damping in MEMS tuning fork resonators," J. Microelectromech. Syst., vol. 27, no. 5, pp. 800–809, Oct. 2018.
- [57] G. D. Vukasin et al., "Effect of substrate thickness on anchor damping in MEMS devices," in Proc. IEEE Transducers Eurosensors, Jun. 2019, pp. 1843–1845.
- [58] J. Rieger, A. Isacsson, M. J. Seitner, J. P. Kotthaus, and E. M. Weig, "Energy losses of nanomechanical resonators induced by atomic force microscopy-controlled mechanical impedance mismatching," *Nature Commun.*, vol. 5, no. 1, pp. 1–6, May 2014.
- [59] A. Rahafrooz and S. Pourkamali, "Thermal-piezoresistive energy pumps in micromechanical resonant structures," *IEEE Trans. Electron Devices*, vol. 59, no. 12, pp. 3587–3593, Dec. 2012.
- [60] K.-H. Li, C.-C. Chen, M.-H. Li, and S.-S. Li, "A self-sustained nanomechanical thermal-piezoresistive oscillator with ultra-low power consumption," in *IEDM Tech. Dig.*, San Francisco, CA, USA, Dec. 2014, pp. 2–22.
- [61] G. Lehee, R. Anciant, F. Souchon, A. Berthelot, P. Rey, and G. Jourdan, "P-type silicon nanogauge based self-sustained oscillator," in *Proc. 19th Int. Conf. Solid-State Sens., Actuators Microsyst.*, Kaohsiung, Taiwan, Jun. 2017, pp. 444–447.
- [62] J. M. L. Miller et al., "Thermal-piezoresistive tuning of the effective quality factor of a micromechanical resonator," *Phys. Rev. Appl.*, vol. 10, no. 4, Oct. 2018, Art. no. 044055.
- [63] A. A. Zope, J.-H. Chang, T.-Y. Liu, and S.-S. Li, "A CMOS-MEMS thermal-piezoresistive oscillator for mass sensing applications," *IEEE Trans. Electron Devices*, vol. 67, no. 3, pp. 1183–1191, Mar. 2020.
- [64] K. Persson. (2014). Materials Data on Si (SG:227) by Materials Project. [Online]. Available: https://materialsproject.org/materials/mp-149/
- [65] K. Persson. (2014). Materials Data on Si₃N₄ (SG:176) by Materials Project. [Online]. Available: https://materialsproject.org/materials/mp-988/
- [66] K. Persson. (2014). Materials Data on LiNbO₃ (SG:161) by Materials Project. [Online]. Available: https://materialsproject.org/materials/mp-3731/
- [67] M. de Jong et al., "Charting the complete elastic properties of inorganic crystalline compounds," Sci. Data, vol. 2, no. 1, pp. 1–13, Dec. 2015.
- [68] J. Xie, Y. Hao, and W. Yuan, "Energy loss in a MEMS disk resonator gyroscope," *Micromachines*, vol. 10, no. 8, p. 493, Jul. 2019.
- [69] R. N. Candler et al., "Single wafer encapsulation of MEMS devices," IEEE Trans. Adv. Packag., vol. 26, no. 3, pp. 227–232, Aug. 2003.
- [70] Y. Yang, E. J. Ng, Y. Chen, I. B. Flader, and T. W. Kenny, "A unified epi-seal process for fabrication of high-stability microelectromechanical devices," *J. Microelectromech. Syst.*, vol. 25, no. 3, pp. 489–497, Jun. 2016.
- [71] J. M. Miller et al., "Thermomechanical-noise-limited capacitive transduction of encapsulated MEM resonators," J. Microelectromech. Syst., vol. 28, no. 6, pp. 965–976, Sep. 2019.
- [72] P. R. Saulson, "Thermal noise in mechanical experiments," Phys. Rev. D, Part. Fields, vol. 42, p. 2437, Oct. 1990.
- [73] H. B. Callen and T. A. Welton, "Irreversibility and generalized noise," Phys. Rev., vol. 83, p. 34, Jul. 1951.
- [74] H. B. Callen and R. F. Greene, "On a theorem of irreversible thermodynamics," *Phys. Rev.*, vol. 86, no. 5, p. 702, 1952.
- [75] M. V. Salapaka, H. S. Bergh, J. Lai, A. Majumdar, and E. McFarland, "Multi-mode noise analysis of cantilevers for scanning probe microscopy," *J. Appl. Phys.*, vol. 81, no. 6, pp. 2480–2487, 1997.

- [76] N. E. Bousse, J. M. L. Miller, H.-K. Kwon, G. D. Vukasin, and T. W. Kenny, "Quality factor tuning of micromechanical resonators via electrical dissipation," *Appl. Phys. Lett.*, vol. 116, no. 2, Jan. 2020, Art. no. 023506.
- [77] T. Middelmann, A. Walkov, G. Bartl, and R. Schödel, "Thermal expansion coefficient of single-crystal silicon from 7 K to 293 K," *Phys. Rev. B, Condens. Matter*, vol. 92, no. 17, pp. 174113-1–174113-7, Nov. 2015.
- [78] E. J. Ng, V. A. Hong, Y. Yang, C. H. Ahn, C. L. M. Everhart, and T. W. Kenny, "Temperature dependence of the elastic constants of doped silicon," *J. Microelectromech. Syst.*, vol. 24, no. 3, pp. 730–741, Jun. 2015.
- [79] F. R. Blom, S. Bouwstra, M. Elwenspoek, and J. H. J. Fluitman, "Dependence of the quality factor of micromachined silicon beam resonators on pressure and geometry," J. Vac. Sci. Technol. B, Microelectron. Nanometer Struct. Process., Meas., Phenomena, vol. 10, no. 1, pp. 19–26, 1992.
- [80] L. G. Villanueva and S. Schmid, "Evidence of surface loss as ubiquitous limiting damping mechanism in SiN micro- and nanomechanical resonators," *Phys. Rev. Lett.*, vol. 113, no. 22, Nov. 2014, Art. no. 227201.
- [81] S. Ghaffari et al., "Quantum limit of quality factor in silicon micro and nano mechanical resonators," Sci. Rep., vol. 3, no. 1, p. 3244, Dec. 2013.
- [82] J. Rodriguez et al., "Direct detection of Akhiezer damping in a silicon MEMS resonator," Sci. Rep., vol. 9, no. 1, p. 2244, Dec. 2019.
- [83] W. A. Phillips, "Two-level states in glasses," Rep. Prog. Phys., vol. 50, no. 12, p. 1657, 1987.
- [84] A. N. Cleland and M. L. Roukes, "External control of dissipation in a nanometer-scale radiofrequency mechanical resonator," Sens. Actuators A, Phys., vol. 72, pp. 256–261, Feb. 1999.
- [85] T. Barois et al., "Ohmic electromechanical dissipation in nanomechanical cantilevers," Phys. Rev. B, Condens. Matter, vol. 85, no. 7, Feb. 2012, Art. no. 075407.
- [86] J. Mertz, O. Marti, and J. Mlynek, "Regulation of a microcantilever response by force feedback," Appl. Phys. Lett., vol. 62, no. 19, pp. 2344–2346, 1993.
- [87] G. Jourdan, G. Torricelli, J. Chevrier, and F. Comin, "Tuning the effective coupling of an AFM lever to a thermal bath," *Nanotechnology*, vol. 18, no. 47, Nov. 2007, Art. no. 475502.



Ze Zhang received the B.S. degree in engineering mechanics from Tsinghua University in 2015 and the M.S. degree in mechanical engineering from Stanford University in 2017. She is currently pursuing the Ph.D. degree with the Department of Mechanical Engineering, Stanford University, working with Prof. Arun Majumdar. Her research interests include nanoscale heat transfer and developing new electron microscopy techniques.



Hyun-Keun Kwon received the B.S. and M.S. degrees in electrical engineering from Korea University, Seoul, Republic of Korea, in 2015, and the Ph.D. degree in mechanical engineering from Stanford University in 2020. Upon graduation, he joined Apple, as a Motion Sensing Hardware Engineer, developing new sensing technology for consumer electronics. His research interests include fabrication process techniques, high-performance ovenized MEM resonator, and MEMS-based timing references.



James M. L. Miller received the B.S. degree in mechanical engineering from Michigan State University in 2014 and the M.S. and Ph.D. degree in mechanical engineering from Stanford University in 2016 and 2021, respectively, with support from the National Defense Science and Engineering (NDSEG) Fellowship and the E. K. Potter Stanford Graduate Fellowship. He is currently a Post-Doctoral Researcher with the Department of Mechanical Engineering and the Department of Physics and Astronomy, Florida Institute of Tech-

nology and Michigan State University. His current research interests include nonlinearities, fluctuations, and dissipation tuning mechanisms in MEM resonators, and parametric interactions in nanophotonic devices.



Gabrielle D. Vukasin received the B.A. degree in astrophysics and mathematics from Williams College in 2014 and the M.S. degree in mechanical engineering from Tufts University in 2016. She is currently pursuing the Ph.D. degree in mechanical engineering from Stanford University. Her research interests include the design and fabrication of MEM resonators with a focus on the characterization of energy loss mechanisms using wide-range temperature measurements of the quality factor.



Arun Majumdar received the B.Tech. degree in mechanical engineering from IIT Bombay in 1985 and the Ph.D. degree in mechanical engineering from the University of California at Berkeley in 1989. He is currently the Jay Precourt Provostial Chair Professor with Stanford University, a Faculty Member of the Department of Mechanical Engineering and the Department of Materials Science and Engineering (by courtesy), and a Senior Fellow and the former Director of the Precourt Institute for Energy. He is also a Faculty with the Department of

Obama and confirmed by the Senate to become the Founding Director of the Advanced Research Projects Agency-Energy (ARPA-E), where he served until June 2012. From March 2011 to June 2012, he also served as the Acting Under Secretary of Energy. After leaving Washington, DC, USA, he was the Vice President for Energy with Google, where he assembled a team to create technologies and businesses at the intersection of data, computing, and electricity grid. Prior to joining the Department of Energy, he was the Almy & Agnes Maynard Chair Professor of mechanical engineering, and materials science and engineering with the University of California-Berkeley and the Associate Laboratory Director for energy and environment with the Lawrence Berkeley National Laboratory. He also spent the early part of his academic career with Arizona State University and the University of California at Santa Barbara. His research in the past has involved the science and engineering of nanoscale materials and devices, especially in the areas of energy conversion, transport, and storage, and biomolecular analysis. His current research focuses on redox reactions and systems that are fundamental to a sustainable energy future, multidimensional nanoscale imaging and microscopy, and an effort to leverage modern AI techniques to develop and deliver energy and climate solutions. He is a member of the U.S. National Academy of Sciences, the U.S. National Academy of Engineering, and the American Academy of Arts and Sciences.

Photon Science, SLAC, In October 2009, he was nominated by the President



Thomas W. Kenny received the B.S. degree from the University of Minnesota in 1983 and the M.S. and Ph.D. degrees from the University of California at Berkeley in 1987 and 1989, respectively, all in physics. From 1989 to 1993, he was with JPL/NASA, Pasadena, CA, USA, where his research focused on the development of electron-tunneling high-resolution microsensors. In 1994, he joined the Department of Mechanical Engineering, Stanford University, Stanford, CA, USA, where he directs microsensor-based research in a variety of areas,

including resonators, wafer-scale packaging, cantilever beam force sensors, microfluidics, and novel fabrication techniques for micromechanical structures. He was the Founder and the CTO of Cooligy (currently a division of Emerson), a microfluidics chip cooling component manufacturer, and the Founder and a Board Member with SiTime Corporation (currently a division of MegaChips), a developer of timing references using MEM resonators. He is also the Founder and a Board Member with Applaud Medical, developing noninvasive therapies for kidney stones. From 2006 to 2010, he served as a Program Manager with the Microsystems Technology Office, DARPA, starting and managing programs in thermal management, nanomanufacturing, manipulation of Casimir forces. He is currently the Richard Weiland Professor of mechanical engineering and the Senior Associate Dean of engineering for student affairs. He has authored or coauthored over 250 scientific articles and holds 50 issued patents, and has been an advisor to over 50 graduated Ph.D. students from Stanford University. He received the Young Faculty Award. He was the General Chairperson of the 2006 Hilton Head Solid-State Sensors, Actuators, and Microsystems Workshop, and the General Chair of the Transducers 2015 Meeting in Anchorage.



Steven W. Shaw received the A.B. degree in physics and the M.S.E. degree in applied mechanics from the University of Michigan in 1978 and 1979, respectively, and the Ph.D. degree in theoretical and applied mechanics from Cornell University in 1983.

He is currently a Harris Professor of mechanical engineering with the Florida Institute of Technology, and the University Distinguished Professor Emeritus of mechanical engineering and an Adjunct Professor of physics and astronomy with Michigan State University. He has held visiting appointments

at Cornell University, the University of Michigan, Caltech, the University of Minnesota, the University of California at Santa Barbara, and McGill University. His research interests include micro/nano-scale resonators and vibration absorbers, with an emphasis on nonlinear behavior. He is a fellow of ASME. He was a recipient of the SAE Arch T. Colwell Merit Award, the Henry Ford Customer Satisfaction Award, the ASME Henry Hess Award, the ASME N. O. Myklestad Award, and the ASME T. K. Caughey Dynamics Award